

Securing the Spike: On the Transferability and Security of Spiking Neural Networks to Adversarial Examples

Nuo Xu*

Lehigh University
nux219@lehigh.edu

Kaleel Mahmood*

University of Connecticut
kaleel.mahmood@uconn.edu

Haowen Fang*

hfang02@syr.edu

Ethan Rathbun

University of Connecticut
ethan.rathbun@uconn.edu

Caiwen Ding

University of Connecticut
caiwen.ding@uconn.edu

Wujie Wen

Lehigh University
wuw219@lehigh.edu

Abstract

Spiking neural networks (SNNs) have attracted much attention for their high energy efficiency and for recent advances in their classification performance. However, unlike traditional deep learning approaches, the analysis and study of the robustness of SNNs to adversarial examples remain relatively underdeveloped. In this work we focus on advancing the adversarial attack side of SNNs and make three major contributions. First, we show that successful white-box adversarial attacks on SNNs are highly dependent on the underlying surrogate gradient technique. Second, using the best surrogate gradient technique, we analyze the transferability of adversarial attacks on SNNs and other state-of-the-art architectures like Vision Transformers (ViTs) and Big Transfer Convolutional Neural Networks (CNNs). We demonstrate that SNNs are not often deceived by adversarial examples generated by Vision Transformers and certain types of CNNs. Third, due to the lack of an ubiquitous white-box attack that is effective across both the SNN and CNN/ViT domains, we develop a new white-box attack, the Auto Self-Attention Gradient Attack (Auto SAGA). Our novel attack generates adversarial examples capable of fooling both SNN models and non-SNN models simultaneously. Auto SAGA is as much as 87.9% more effective on SNN/ViT model ensembles than conventional white-box attacks like PGD. Our experiments and analyses are broad and rigorous covering three datasets (CIFAR-10, CIFAR-100 and ImageNet), five different white-box attacks and nineteen different classifier models (seven for each CIFAR dataset and five different models for ImageNet).

*These authors contributed equally to this work.

1. Introduction

There is an increasing demand to deploy machine intelligence to power-limited scenarios such as mobile electronics and Internet-of-Things (IoT), however the computation complexity of deep learning models, coupled with energy consumption has become a challenge [23, 39]. This motivates a new computing paradigm, bio-inspired energy efficient neuromorphic computing. As the underlying computational model, Spiking Neural Networks (SNNs) have drawn considerable interest [7, 39]. SNNs can provide high energy efficient solutions for resource-limited applications. For example, in [43] an SNN was used for a robot navigation task with Intel’s Loihi [6] and achieved a $276\times$ reduction in energy as compared to a conventional machine learning approach. In [36] it was reported that an SNN consumed $0.66mJ$, $102mJ$ per sample on MNIST and CIFAR 10, while a DNN consumed $111mJ$ and $1035mJ$, resulting in $168\times$ and $10\times$ energy reduction, respectively. Emerging SNN techniques such as joint thresholding, leakage, and weight optimization using surrogate gradients have all led to improved performance. Both transfer based [27, 34, 35] SNNs and Backpropagation (BP) trained-from-scratch SNNs [13–15, 40] achieve similar performance to DNNs, while at the same time using significantly less energy.

On the other hand, the vulnerability of deep learning models to adversarial examples [17] is one of the main topics that has received much attention in recent research. An adversarial example is an input that has been manipulated with a small amount of noise such that a human being can correctly classify it (i.e if the input is an image). However, the adversarial example is misclassified by a machine learning model with high confidence. A large body of literature has been devoted to the development of both adversarial attacks [45] and defenses [50] for CNNs.

As SNNs become more accurate and more widely adopted, their security vulnerabilities will emerge as an important issue. Recent work has been done to study some of the security aspects of the SNN [11, 16, 24, 25, 37, 38], although not to the same extent as CNNs. To the best of our knowledge, there has not been rigorous analyses done on how the different choice of gradient estimations can effect white-box SNN attacks, whether SNN adversarial examples are misclassified by other state-of-the-art models like Vision Transformers and finally there has not been any general attack method developed to break both SNNs and CNNs/ViTs simultaneously.

With these goals, we first need to explore the attack effectiveness of existing white-box attacks on SNNs. Specifically, do factors like the choice of surrogate gradient estimator effect the white-box attack success rate? In addition to this, the transferability of attacks between different kinds of neural networks is important to ensure the generality of the attacks. Previous works [26, 31, 33] have explored the transferability between CNNs and Vision Transformers, we extend these analyses to both BP and transfer based SNNs. Thus in our paper, we specifically focus on three key adversarial aspects:

1. *How are white-box attacks on SNNs affected by different SNN surrogate gradient estimation techniques?*
2. *As SNNs have shown more robustness in previous studies [25, 37], do adversarial examples generated by SNNs transfer to other models such as Vision Transformers and CNNs and vice versa?*
3. *Are there white-box attacks capable of bridging the transferability gap and achieving a high attack success rate against both SNNs and CNNs or Vision Transformers?*

To address these questions and advance the field of adversarial machine learning we organize the rest of our paper as follows: in Section 2 we briefly introduce the different types of SNNs (BP and Transfer) whose security we analyze. In Section 3 we analyze the effect of seven different surrogate gradient estimators on the attack success rate of white-box adversarial attacks. We show that the choice of surrogate gradient estimator is highly influential and must be carefully selected. In Section 4 we use the best surrogate gradient estimator to study the transferability of adversarial examples generated by SNNs, Vision Transformers and various CNN models. We analyze the misclassification rates of adversarial examples between 12 different models on CIFAR-10 (and provide related CIFAR-100 results in the Appendix). Our transferability experiments demonstrate that traditional white-box attacks do not work well on both SNNs and other models like Vision Transformers simultaneously. This result creates the opportunity for

the development of an attack capable of breaking multiple models. To this end, we propose a new multi-model attack in Section 5 called the Auto Self-Attention Gradient Attack (Auto-SAGA) capable of creating adversarial examples that are misclassified by both SNN and non-SNN models.

Overall, we conduct rigorous analyses and experiments with 19 different models across three datasets (CIFAR-10, CIFAR-100 and ImageNet). Our surrogate gradient and transferability results yield new insights into SNN security. Our newly proposed attacks (Auto-SAGA) works on SNN/ViT/CNN ensembles and shows a higher attack success rate (as much as 87.9% improvement) over conventional white-box attacks. In short, all three of our major paper contributions advance the attack development of SNN adversarial machine learning.

2. SNN Models

In this section, we discuss the basics of the SNN architecture and of neural encoding. Widely used Leaky Integrate and Fire (LIF) neuron can be described by a system of difference equations as follows [39]:

$$V[t] = \alpha V[t-1] + \sum_i w_i S_i[t] - \vartheta O[t-1] \quad (1a)$$

$$O[t] = u(V[t] - \vartheta) \quad (1b)$$

$$u(x) = 0, x < 0 \text{ otherwise } 1 \quad (1c)$$

where $V[t]$ denotes neuron’s membrane potential. $\alpha \in (0, 1]$ is a time constant, which controls the decay speed of membrane potential. When $\alpha = 1$, $V[t]$ no longer decays over time, the model becomes Integrate and Fire (IF) neuron. $S_i[t]$ and w_i are i_{th} input and the associated weight. ϑ is the neuron’s threshold, $O[t]$ is the neuron’s output function, $u(\cdot)$ is the Heaviside step function. If membrane potential $V[t]$ is greater than the threshold ϑ , the neuron will fire a spike, hence $O[t]$ will be 1. Then, at the next time step, $V[t]$ will be decreased by ϑ in a procedure referred to as a reset [39].

Note that, in contrast to the continuous input domains of DNNs, in SNNs information is represented by discrete, binary spike trains. Therefore, data has to be mapped to spike domain for an SNN to process, this procedure is referred to as neural encoding, which plays an essential role in high performance SNN applications [39]. A popular way to achieve such mapping is the direct encoding [34, 47]. This method uses Current-Based neuron (CUBA) as the first layer in an SNN’s architecture. CUBA accepts continuous value instead of spikes [12] such that a pixel value can be converted into spike train and then directly fed to the SNN. Because direct encoding can reduce inference latency by a factor of 5–100 [34], recent works have achieved state-of-the-art results with this coding scheme [13, 14, 24, 34], all experiments employ direct coding in this work.

2.1. SNN Training

Spiking neuron’s non-differentiable activation makes directly applying BP difficult [14,25,44,51]. Training an SNN requires different approaches, which can be categorized as follows:

Conversion-based training. A common practice is to use spike numbers in a fixed time window (spike rate) to represent a numerical value. The input strength and neuron’s spike rate roughly have a linear relation, such behavior is similar to ReLU function in DNNs [8]. Therefore it is possible to pretrain a DNN model and map the weights to an SNN. However, simply mapping the weights suffers from performance degradation due to non-ideal input-spike rate linearity, over activation, and under activation [8,34]. Additional post-processing and fine tuning are required to compensate for the performance degradation. In [8] they propose weight-threshold balancing which scales the weights by a certain factor to recover accuracy. In [34] they use pre-trained DNN weights as initialization and then retrain the SNN to reduce accuracy degradation.

Surrogate gradient-based BP. Equation 1a - 1c reveal that SNNs have similar form as Recurrent Neural Networks (RNNs). The output, membrane potential are dependent on input and historical states. Equation 1a is actually differentiable, thereby making it possible to unfold the SNN and use BP to train it. The challenge is Equation 1c, i.e. the Heaviside step function $u(\cdot)$ is non-differentiable. To overcome this issue, the surrogate gradient method has been proposed, which allows the Heaviside step function’s derivative to be approximated by some smooth functions. In forward pass, the spike is still generated by $u(\cdot)$, in the backward pass the gradient is approximated by a surrogate gradient as if $u(\cdot)$ is differentiable. Using a surrogate gradient enables SNN training with BP from scratch and achieves comparable performance to DNNs [14, 40]. The choice of surrogate gradients is flexible. Hence, this raises an important question about which surrogate gradient method to use in BP for white-box adversarial attacks. We investigate this question in Section 3.

3. SNN Surrogate Gradient Estimation

Do different SNN surrogate gradient estimators effect white-box attack success rate? In both neural network training and white-box adversarial machine learning attacks the fundamental computation requires backpropagating through the model. Due to the non-differentiable structure of SNNs [32], this requires using a surrogate gradient estimator. In [49] it was shown that gradient based SNN training was robust to different derivative shapes. In [47] it was shown that there are multiple different surrogate gradient estimators which can lead to reasonably good performance on MNIST, Neuromorphic-MNIST and CIFAR 10.

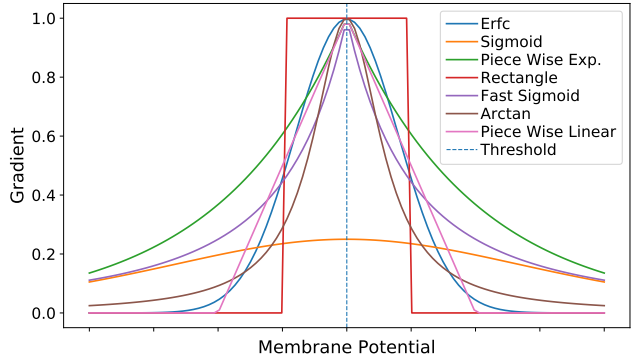


Figure 1. Different surrogate gradient functions.

While there exist multiple surrogate gradient estimators for SNN training, in the field of adversarial machine learning, precise gradient calculations are paramount. Incorrect gradient estimation on models leads to a phenomenon known as gradient masking [2]. Models that suffer from gradient masking appear robust, but only because the model gradient is incorrectly calculated in white-box attacks performed against them. This issue has led to many published models and defenses to claim security, only to later be broken when correct gradient estimators were implemented [45]. To the best of our knowledge, this issue has not been thoroughly explored for SNNs in the context of adversarial examples. Thus we pose the fundamental question: Do different SNN surrogate gradient estimators effect white-box attack success rate?

3.1. Surrogate Gradient

Surrogate gradient [32] has become a popular technique to overcome the non-differentiable problem of spiking neuron’s binary activation. Let $u(x)$ be Heaviside step function, and $u'(x)$ be its derivative. The surrogate gradients investigated in this work are discussed as follows:

Sigmoid [4] indicates that a hard threshold function’s derivative can be approximated by that of a sigmoid function. The surrogate gradient is given by Equation 2:

$$u'(x) \approx \frac{e^{\vartheta-x}}{(1 + e^{\vartheta-x})^2} \quad (2)$$

Erfc [13] proposes to use the Poisson neuron’s spike rate function. The spike rate can be characterized by complementary error function (erfc), and its derivative is calculated as Equation 3, where σ controls the sharpness:

$$u'(x) \approx \frac{e^{-\frac{(\vartheta-x)^2}{2\sigma^2}}}{\sqrt{2\pi}\sigma} \quad (3)$$

Arctan [15] uses gradient of arctangent function as sur-

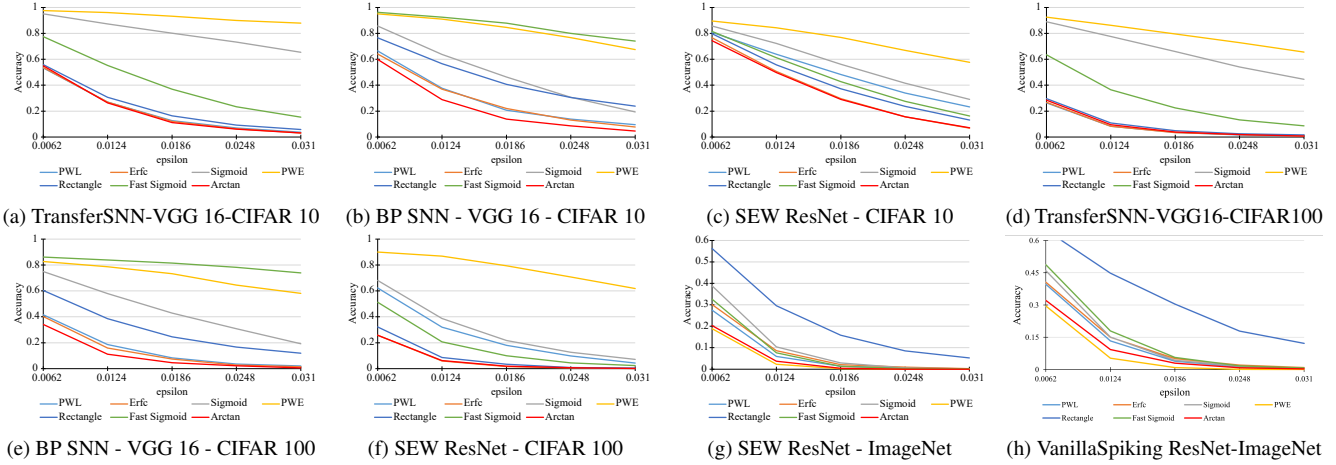


Figure 2. White-box attack on three SNN models using different surrogate gradients. (a) (b) (c) indicate results on CIFAR-10, (d) (e) (f) indicates results on CIFAR-100, and (g) (h) is result on ImageNet. Every curve corresponds to the performance of attack with a surrogate gradient. y-axis is accuracy, x-axis is epsilon.

rogate gradient, which is given by:

$$u'(x) \approx \frac{1}{1 + \pi^2(x - \vartheta)^2} \quad (4)$$

Piece-wise linear function (PWL) There are various works use PWL function as gradient surrogate [3, 32, 34]. Its formulation is given below:

$$u'(x) \approx \max(0, 1 - |x|) \quad (5)$$

Fast sigmoid [48] uses fast sigmoid as a replacement of the sigmoid function, the purpose is to avoid expensive exponential operation and to speed up computation.

$$u'(x) \approx \frac{1}{1 + (1 + |x - \vartheta|)^2} \quad (6)$$

Piece-wise Exponential [40] suggests that Probability Density Function (PDF) for a spiking neuron to change its state (fire or not) can approximate the derivative of the spike function. Spike Escape Rate, which is a piece-wise exponential function, can be a good candidate to characterize this probability density. It is given by Equation 7

$$u'(x) \approx \frac{1}{\alpha e^{-\beta|x-\vartheta|}} \quad (7)$$

where α and β are two hyperparameters.

Rectangular function is used by [46, 47] as surrogate gradient. α is a hyperparameter that controls height and width.

$$u'(x) \approx \frac{1}{\alpha} \text{sign}(|v - \vartheta| < \frac{\alpha}{2}) \quad (8)$$

| CIFAR 10 | | | | | |
|-----------------|------------|--------|--------|--------|-------|
| | ϵ | | | | |
| Surrogate Grad. | 0.0062 | 0.0124 | 0.0186 | 0.0248 | 0.031 |
| PWL | 53.3% | 26.9% | 12.6% | 7.0% | 3.7% |
| Erfc | 53.7% | 26.9% | 12.0% | 6.4% | 3.2% |
| Sigmoid | 95.1% | 8.72% | 80.1% | 73.3% | 65.4% |
| Piecewise Exp. | 97.5% | 96.0% | 93.2% | 90.0% | 87.9% |
| Rectangle | 55.8% | 30.7% | 16.4% | 9.2% | 5.8% |
| Fast Sigmoid | 77.4% | 55.3% | 37.0% | 23.4% | 15.3% |
| Arctan | 55.0% | 26.4% | 11.2% | 6.1% | 3.1% |

| CIFAR 100 | | | | | |
|-----------------|------------|--------|--------|--------|-------|
| | ϵ | | | | |
| Surrogate Grad. | 0.0062 | 0.0124 | 0.0186 | 0.0248 | 0.031 |
| PWL | 26.4% | 8.4% | 3.5% | 1.7% | 1.0% |
| Erfc | 26.9% | 8.4% | 3.4% | 2.0% | 0.9% |
| Sigmoid | 88.9% | 77.6% | 66.0% | 54.0% | 44.5% |
| Piecewise Exp. | 92.5% | 86.2% | 79.5% | 7.28% | 65.5% |
| Rectangle | 29.7% | 10.9% | 4.9% | 2.5% | 1.7% |
| Fast Sigmoid | 63.4% | 36.5% | 22.5% | 13.2% | 8.7% |
| Arctan | 28.5% | 9.6% | 3.8% | 1.9% | 0.8% |

Table 1. White box attack success rate for transfer SNN VGG 16 model on CIFAR 10 and CIFAR 100 with respect to different surrogate gradients.

3.2. Surrogate Gradient Estimator Experiments

Experimental Setup: We evaluate the attack success rate of 3 types of SNN on CIFAR-10/100 and 2 types of SNN on ImageNet using 7 different surrogate gradient estimators. For the attack we use one of the most common white-box attacks, the Projected Gradient Descent (PGD) attack with respect to the l_∞ norm. In terms of SNN models we test the Transfer SNN VGG-16 [34], the BP SNN VGG-16 [13], a Spiking Element Wise (SEW) ResNet [14], and

| CIFAR 10 | | | | | |
|-----------------|------------|--------|--------|--------|-------|
| | ϵ | | | | |
| Surrogate Grad. | 0.0062 | 0.0124 | 0.0186 | 0.0248 | 0.031 |
| PWL | 66.5% | 37.7% | 20.7% | 13.9% | 9.5% |
| Erfc | 64.1% | 37.0% | 22.1% | 13.1% | 7.7% |
| Sigmoid | 85.7% | 63.7% | 46.3% | 30.7% | 19.4% |
| Piecewise Exp. | 95.1% | 91.0% | 84.6% | 76.7% | 67.5% |
| Rectangle | 76.5% | 56.6% | 40.6% | 30.5% | 23.9% |
| Fast Sigmoid | 96.3% | 92.5% | 87.9% | 80.0% | 74.1% |
| Arctan | 59.9% | 28.9% | 13.9% | 8.6% | 4.6% |

| CIFAR 100 | | | | | |
|-----------------|------------|--------|--------|--------|-------|
| | ϵ | | | | |
| Surrogate Grad. | 0.0062 | 0.0124 | 0.0186 | 0.0248 | 0.031 |
| PWL | 41.6% | 18.6% | 8.4% | 3.6% | 2.1% |
| Erfc | 40.2% | 16.0% | 7.4% | 2.9% | 1.5% |
| Sigmoid | 75.0% | 58.0% | 42.9% | 30.9% | 19.3% |
| Piecewise Exp. | 82.7% | 78.7% | 73.2% | 64.5% | 58.1% |
| Rectangle | 60.4% | 38.6% | 24.5% | 16.7% | 11.9% |
| Fast Sigmoid | 86.1% | 83.8% | 81.5% | 78.2% | 73.9% |
| Arctan | 34.2% | 11.2% | 4.6% | 2.2% | 0.6% |

Table 2. White box attack success rate for BP SNN VGG 16 model on CIFAR 10 and CIFAR 100 with respect to different surrogate gradients.

Vanilla Spiking ResNet [52]. The surrogate gradients investigated in this works are: sigmoid [32], erfc [13], piece-wise linear (PWL) [34], piece-wise exponential (PWE) [40], rectangle [46], fast sigmoid [48] and arctangent [14]. The shapes of these surrogate gradient functions are shown in Figure 1. Detailed mathematical descriptions of the gradient estimators are provided in our Appendix. When conducting PGD, we keep the models forward pass unchanged, and the surrogate gradient function is substituted in the backward pass only. In training phase, we use the same surrogate gradient settings as original works, which are erfc for BP SNN Vgg-16, PWL for transfer SNN VGG-16, arctangent for SEW ResNet and Vanilla Spiking ResNet.

Experimental Analysis: The results of our surrogate gradient estimation experiments are shown in Figure 2 (full numerical tables are shown in Table 1, 2, 3, and 4). For each model and each gradient estimator, we vary the maximum perturbation bounds from $\epsilon = 0.0062$ to $\epsilon = 0.031$ on the x-axis and run the PGD attack on 1000 (CIFAR 10 and CIFAR 100), and 2000 (ImageNet) clean, correctly identified and class-wise balanced samples from the validation set. The corresponding robust accuracy is then measured on the y-axis. Our results show that unlike what the literature reported for SNN training [47], the choice of surrogate gradient estimator hugely impacts SNN attack performance. In most cases the arctan performs best (except for the case of ImageNet, arctan is the second best, performance is slightly lower than PWE). To reiterate, this set of experiments highlights a significant finding: *gradient masking can occur in*

| CIFAR 10 | | | | | |
|-----------------|------------|--------|--------|--------|-------|
| | ϵ | | | | |
| Surrogate Grad. | 0.0062 | 0.0124 | 0.0186 | 0.0248 | 0.031 |
| PWL | 80.7% | 63.9% | 48.3% | 34.0% | 23.3% |
| Erfc | 76.5% | 50.6% | 29.6% | 15.6% | 06.8% |
| Sigmoid | 85.6% | 72.2% | 56.1% | 41.5% | 29.0% |
| Piecewise Exp. | 89.6% | 84.3% | 76.8% | 66.8% | 57.7% |
| Rectangle | 79.7% | 55.7% | 37.3% | 23.7% | 13.1% |
| Fast Sigmoid | 81.5% | 61.2% | 42.8% | 27.6% | 16.2% |
| Arctan | 74.4% | 49.7% | 29.0% | 15.6% | 7.2% |

| CIFAR 100 | | | | | |
|-----------------|------------|--------|--------|--------|-------|
| | ϵ | | | | |
| Surrogate Grad. | 0.0062 | 0.0124 | 0.0186 | 0.0248 | 0.031 |
| PWL | 62.3% | 32.0% | 18.0% | 9.9% | 4.4% |
| Erfc | 25.8% | 5.9% | 1.7% | 0.6% | 0.2% |
| Sigmoid | 68.1% | 38.7% | 21.8% | 12.6% | 07.2% |
| Piecewise Exp. | 90.0% | 86.9% | 79.4% | 70.8% | 61.9% |
| Rectangle | 32.2% | 8.7% | 3.4% | 0.9% | 0.4% |
| Fast Sigmoid | 51.2% | 20.7% | 10.0% | 4.5% | 2.4% |
| Arctan | 25.8% | 6.3% | 1.9% | 0.7% | 0.2% |

| ImageNet | | | | | |
|-----------------|------------|--------|--------|--------|-------|
| | ϵ | | | | |
| Surrogate Grad. | 0.0062 | 0.0124 | 0.0186 | 0.0248 | 0.031 |
| PWL | 27.5% | 5.9% | 1.4% | 0.45% | 0.1% |
| Erfc | 30.1% | 8.6% | 2.05% | 0.95% | 0.25% |
| Sigmoid | 38.85% | 10.35% | 2.9% | 0.6% | 0.1% |
| Piecewise Exp. | 18.85% | 2.25% | 0.25% | 0.05% | 0.05% |
| Rectangle | 56.25% | 29.55% | 15.85% | 8.55% | 5.25% |
| Fast Sigmoid | 32.65% | 7.65% | 1.3% | 0.3% | 0.15% |
| Arctan | 20.3% | 3.65% | 0.35% | 0% | 0% |

Table 3. White box attack success rate for SEW ResNet 18 model on CIFAR 10, CIFAR 100 and ImageNet with respect to different surrogate gradients.

| ImageNet | | | | | |
|-----------------|------------|--------|--------|--------|--------|
| | ϵ | | | | |
| Surrogate Grad. | 0.0062 | 0.0124 | 0.0186 | 0.0248 | 0.031 |
| PWL | 39.65% | 13.3% | 3.9% | 1.4% | 0.55% |
| Erfc | 40.65% | 15.05% | 5.1% | 2.05% | 0.95% |
| Sigmoid | 46.0% | 15.15% | 4.35% | 0.155% | 0.25% |
| Piecewise Exp. | 29.60% | 5.3% | 0.9% | 0.1% | 0% |
| Rectangle | 64.95% | 44.8% | 30.5% | 17.9% | 12.15% |
| Fast Sigmoid | 48.8% | 17.95% | 5.7% | 1.7% | 0.75% |
| Arctan | 32.2% | 9.3% | 3.0% | 0.85% | 0.3% |

Table 4. White box attack success rate for Vanilla Spiking ResNet 18 model on ImageNet with respect to different surrogate gradients.

SNNs if an improper surrogate gradient estimator is used. For the remainder of the paper our white-box attacks all use the arctan surrogate gradient estimator to maximize the attack success rate.

4. SNN Transferability Study

In this section, we investigate two fundamental security questions pertaining to SNNs. First, *how vulnerable are*

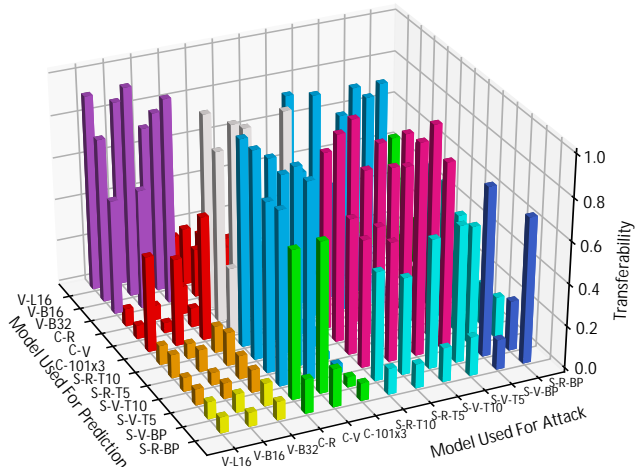


Figure 3. Visual representation of Table 6 for CIFAR-10. The x-axis corresponds to the model used to generate the adversarial examples. The y-axis corresponds to the model used to classify the adversarial examples. The z-axis corresponds to the transferability measurement (see Equation 11). The colors of the bars represent the measurements between different model types, e.g. yellow represents the transferability results between BP SNNs and ViTs.

SNNs to adversarial examples generated from other machine learning models? Second, do non-SNN models misclassify adversarial examples created from SNNs?

Formally, the concept of adversarial examples that are misclassified by multiple models is called, *transferability*. For CNN models, the transferability of adversarial examples was first shown in [42]. Further studies have been done on the transferability of adversarial examples between CNNs with different architectures in [26] and on the transferability between ViTs and CNNs in [30]. To the best of our knowledge, the transferability of SNN adversarial examples when compared to state-of-art architectures like Big Transfer Models [20] and Vision Transformers [10] has never been done.

4.1. Adversarial Example Transferability

In this subsection we briefly define how the transferability between machine learning models is measured. To begin consider a white-box attack A on classifier C_i which produces adversarial example x_{adv} :

$$x_{adv} = A_{C_i}(x, t) \quad (9)$$

where x is the original clean example and t is the corresponding correct class label. Now consider a second classifier C_j independent from classifier C_i . The adversarial example x_{adv} transfers from C_i to C_j if and only if the original clean example x is correctly identified by C_j and x_{adv} is misclassified by C_j :

$$\{C_j(x) = t\} \wedge \{C_j(x_{adv}) \neq t\} \quad (10)$$

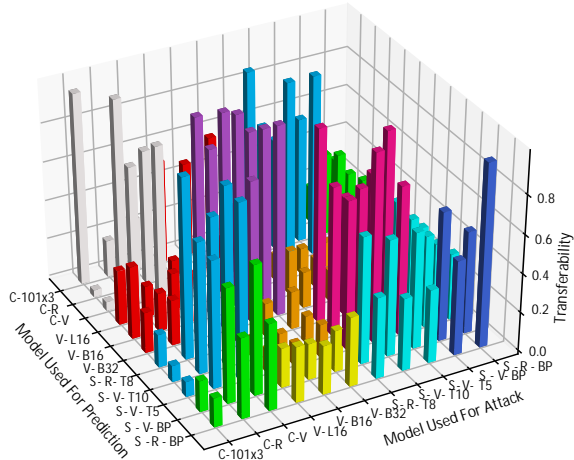


Figure 4. Visual representation of Table 7 for CIFAR-100. The x-axis corresponds to the model used to generate the adversarial examples. The y-axis corresponds to the model used to classify the adversarial examples. The z-axis corresponds to the transferability measurement (see Equation 11). The colors of the bars represent the measurements between different model types, e.g. yellow represents the transferability results between BP SNNs and ViTs.

We can further expand Equation 10 to consider multiple (n) adversarial examples:

$$T_{i,j} = \frac{1}{n} \sum_{k=1}^n \begin{cases} 1 & \text{if } C_j(A_{C_i}(x_k, t_k)) \neq t_k, \\ 0 & \text{otherwise.} \end{cases} \quad (11)$$

From Equation 11 we can see that a high transferability suggests models share a security vulnerability, that is, most of the adversarial examples are misclassified by both models C_i and C_j .

4.2. Transferability Experiment and Analysis

Experimental Setup: For our transferability experiment we analyze three common white-box adversarial attacks which have been experimentally verified to exhibit transferability [29]. The three attacks are the Fast Gradient Sign Method (FGSM) [16], Projected Gradient Descent (PGD) [28] and the Momentum Iterative Method (MIM) [9]. For each attack we use the l_∞ norm with $\epsilon = 0.031$. For brevity, we only list the main attack parameters here and give detailed descriptions of the attacks in our Appendix. When running the attacks on SNN models we use the best surrogate gradient function (Arctan) as demonstrated in Section 3.

In terms of datasets, we show results for CIFAR-10 here and present the CIFAR-100 results (which exhibit a similar trend) in the Appendix. When running the transferability experiment between two models, we randomly select 1000 clean examples that are correctly identified by both models and class-wise balanced.

| | CIFAR-10 | | CIFAR-100 |
|---------|----------|---------|-----------|
| S-R-BP | 81.1% | S-R-BP | 65.1% |
| S-V-BP | 89.2% | S-V-BP | 64.1% |
| S-V-T5 | 90.9% | S-V-T5 | 65.8% |
| S-V-T10 | 91.4% | S-V-T10 | 65.4% |
| S-R-T5 | 89.2% | S-R-T8 | 59.7% |
| S-R-T10 | 91.6% | - | - |
| C-101x3 | 98.7% | C-101x3 | 91.8% |
| C-V | 91.9% | C-V | 66.6% |
| C-R | 92.1% | C-R | 61.3% |
| V-B32 | 98.6% | V-B32 | 91.7% |
| V-B16 | 98.9% | V-B16 | 92.8% |
| V-L16 | 99.1% | V-L16 | 94.0% |

Table 5. Clean Accuracy for models for CIFAR-10 and CIFAR-100 datasets.

Models: To study the transferability of SNNs in relation to other models we use a wide range of classifiers. These include Vision Transformers: ViT-B-32, ViT-B-16 and ViT-L-16 [10]. We also employ a diverse group of CNNs: VGG-16 [41], ResNet-20 [18] and BiT-101x3 [20]. For SNNs we use both BP and Transfer trained models. For BP SNNs we experiment with [13, 14]. For Transfer SNNs we study [34]. We summarise the clean accuracy for all models we used in evaluation in Table 5.

Experimental Analysis: The results of our transferability study for CIFAR-10 are given in Table 6 where each entry in Table 6 corresponds to the maximum transferability attack result measured across FGSM, PGD and MIM. The full transferability results for three attacks are given Table 14 in Appendix C. Figure 3 is a visual representation of Table 6. In Figure 3 the x-axis corresponds to the model used to generate the adversarial example (C_i in Equation 11) and the y-axis corresponds to the model used to classify the adversarial example (C_j in Equation 11). Lastly, the colored bar corresponds to the transferability measurement ($T_{i,j}$ in Equation 11). A higher bar means that a large percentage of the adversarial examples are misclassified by both models. The results for CIFAR100 exhibit a similar trend, see Table 7 with the corresponding visualization in Figure 4 and full transferability results in Table 15 in Appendix C.

Due to the unprecedented scale of our study (12 models with 144 transferability measurements), the results presented in Table 6 and Figure 3 reveal many interesting trends. We will summarize the main trends here (and discuss other findings in the Appendix):

1. *All types of SNNs and ViTs have remarkably low transferability.* In Figure 3 the yellow bars represent the transferability between BP SNNs and ViTs and the orange bars represent the transferability between Transfer SNNs and ViTs. We can clearly see adversarial ex-

amples do not transfer between the two. For example, the SEW ResNet (S-B-RN in Table 6) misclassifies adversarial examples generated by ViT-L-16 (V-L16 in Table 6) only 4.4% of the time.

Likewise, across all ViT models that evaluate adversarial examples created by SNNs the transferability is also low. The maximum transferability for this type of pairing occurs between ViT-B-32 (V-B32 in Table 6) and the Transfer SNN ResNet with timestep 10 (S-T10-RN in Table 6) at a low 15.9%.

2. *Transfer SNNs and CNNs have high transferability, but BP SNNs and CNNs do not* In Figure 3 the blue bars represent the transferability between Transfer SNNs and CNNs which we can visually see is large. For example, 94.1% of the time the Transfer SNN ResNet with timestep 10 (S-R-T10 in Table 6) misclassifies adversarial examples created by the CNN ResNet (C-R in Table 6). This is significant because it highlights that even though the structure of the SNN is fundamentally different from the CNN, when weight transfer training is done, both models still share the same vulnerabilities. The exception to this trend is the CNN BiT-101x3 (C-101x3 in Table 6). We hypothesize that the low transferability of this model with SNNs occurs due to the difference in training (BiT-101x3 is pre-trained on ImageNet-21K and uses a non-standard image size (160x128) in our implementation.

Overall our transferability study demonstrates the fact that there exists multiple model pairings between SNNs, ViTs and CNNs that exhibit the low transferability phenomena for FGSM, PGD and MIM adversarial attacks.

5. Transferability and Multi-Model Attacks

Can different types of models be combined to achieve robustness? In the previous section, we demonstrated that the transferability of adversarial examples between SNNs and other model types was remarkably low. For example, adversarial examples generated from SNNs are not often misclassified by ViT models and vice versa. A natural question arises from this observation: Can different models with low transferability be combined to achieve robustness? This question seems to indicate multi-models with low transferability can provide security. As demonstrated in Section 5, FGSM, MIM and PGD adversarial examples don't transfer well between SNNs, ViTs and CNNs. However, it is important to note that these attacks are designed for single models. A truly robust defense needs to be tested against attacks that work on multiple models. One of the most recent state-of-the-art attacks to bridge the transferability gap is the Self-Attention Gradient Attack (SAGA) proposed in [30].

| | S-R-BP | S-V-BP | S-V-T5 | S-V-T10 | S-R-T5 | S-R-T10 | C-101x3 | C-V | C-R | V-B32 | V-B16 | V-L16 |
|---------|--------|--------|--------|---------|--------|---------|---------|-------|-------|-------|-------|-------|
| S-R-BP | 69.2% | 23.7% | 19.5% | 19.9% | 26.1% | 22.4% | 5.3% | 18.0% | 21.6% | 7.5% | 6.1% | 4.4% |
| S-V-BP | 14.2% | 80.2% | 55.9% | 55.4% | 65.1% | 67.3% | 11.6% | 54.2% | 64.4% | 10.3% | 9.3% | 5.0% |
| S-V-T5 | 18.5% | 64.9% | 88.3% | 100.0% | 85.1% | 85.0% | 16.6% | 97.7% | 86.0% | 10.5% | 12.6% | 9.0% |
| S-V-T10 | 16.3% | 61.3% | 99.8% | 83.2% | 77.4% | 83.2% | 13.8% | 98.1% | 79.9% | 9.6% | 11.7% | 8.3% |
| S-R-T5 | 11.5% | 46.1% | 56.7% | 58.0% | 78.7% | 96.7% | 16.6% | 55.3% | 91.9% | 10.3% | 12.6% | 7.9% |
| S-R-T10 | 12.4% | 51.7% | 60.5% | 64.5% | 97.7% | 83.9% | 20.2% | 63.5% | 94.1% | 11.7% | 11.2% | 8.1% |
| C-101x3 | 8.4% | 4.8% | 4.4% | 3.6% | 8.8% | 6.0% | 100.0% | 2.5% | 3.8% | 8.5% | 21.5% | 11.5% |
| C-V | 18.2% | 71.3% | 92.7% | 93.7% | 84.5% | 86.4% | 26.9% | 89.3% | 85.7% | 20.9% | 22.8% | 16.2% |
| C-R | 16.4% | 70.2% | 82.3% | 80.3% | 98.1% | 97.7% | 31.6% | 81.0% | 92.9% | 23.0% | 27.2% | 17.5% |
| V-B32 | 8.8% | 10.9% | 10.8% | 11.2% | 15.9% | 12.7% | 58.7% | 9.2% | 13.5% | 97.1% | 85.3% | 72.7% |
| V-B16 | 6.7% | 8.9% | 7.5% | 6.0% | 10.6% | 7.2% | 41.4% | 4.9% | 7.1% | 56.7% | 99.6% | 87.5% |
| V-L16 | 7.6% | 8.2% | 7.7% | 6.7% | 11.2% | 9.2% | 45.4% | 6.5% | 8.4% | 54.4% | 77.8% | 92.8% |

Table 6. Transferability results for CIFAR-10. The first column in represents the model used to generate the adversarial examples, C_i . The top row in represents the model used to evaluate the adversarial examples, C_j . Each entry is the maximum transferability computed using C_i and C_j with three different white-box attacks, MIM, PGD and FGSM using Equation 15. Transferability results for other datasets are given in the Appendix. Model abbreviations are used for succinctness, S=SNN, R=ResNet, V=VGG-16, C=CNN, BP=Backpropagation, T denotes the Transfer SNN model with corresponding timestep and V=ViT.

| | S-R-BP | S-V-BP | S-V-T5 | S-V-T10 | S-R-T8 | V-B32 | V-B16 | V-L16 | C-V | C-R | C-101x3 |
|---------|--------|--------|--------|---------|--------|-------|-------|-------|-------|-------|---------|
| S-R-BP | 94.4% | 52.8% | 34.2% | 32.4% | 33.8% | 30.8% | 28.8% | 22.8% | 31.8% | 28.6% | 29.6% |
| S-V-BP | 48.8% | 66.6% | 47.2% | 49.0% | 51.0% | 18.2% | 21.2% | 14.4% | 48.8% | 42.2% | 18.4% |
| S-V-T5 | 37.8% | 60.0% | 76.4% | 97.4% | 69.4% | 18.8% | 19.8% | 13.0% | 93.0% | 64.4% | 20.8% |
| S-V-T10 | 37.4% | 60.0% | 96.8% | 72.0% | 60.6% | 15.6% | 14.8% | 13.2% | 93.0% | 57.0% | 19.8% |
| S-R-T8 | 41.8% | 65.4% | 76.4% | 76.4% | 99.0% | 18.6% | 22.8% | 13.4% | 73.6% | 95.4% | 18.6% |
| V-B32 | 35.8% | 21.4% | 17.0% | 14.0% | 19.4% | 97.4% | 89.2% | 81.2% | 12.8% | 12.0% | 58.8% |
| V-B16 | 25.2% | 18.6% | 11.0% | 8.8% | 17.2% | 73.2% | 99.8% | 94.4% | 8.4% | 6.0% | 48.6% |
| V-L16 | 28.8% | 20.4% | 12.0% | 10.6% | 17.6% | 66.2% | 86.0% | 95.6% | 9.0% | 7.8% | 53.2% |
| C-V | 44.6% | 66.8% | 90.4% | 91.8% | 69.4% | 30.0% | 24.8% | 19.0% | 78.0% | 69.0% | 26.8% |
| C-R | 41.6% | 59.2% | 65.6% | 67.6% | 92.8% | 23.4% | 19.8% | 16.2% | 71.0% | 98.6% | 19.0% |
| C-101x3 | 15.0% | 16.0% | 7.8% | 8.4% | 17.0% | 21.0% | 37.4% | 28.2% | 4.6% | 3.6% | 98.6% |

Table 7. Transferability results for CIFAR-100. The first column in each table represents the model used to generate the adversarial examples, C_i . The top row in each table represents the model used to evaluate the adversarial examples, C_j . Each entry is the maximum transferability computed using C_i and C_j with three different white-box attacks, MIM, PGD and FGSM using Equation 15. Model abbreviations are used for succinctness, S=SNN, -R=ResNet, -V=VGG-16, C=CNN, BP=Backpropagation, T denotes the Transfer SNN model with corresponding timestep and V=ViT.

5.1. The Self-Attention Gradient Attack

In SAGA, the goal of the attacker is to create an adversarial example misclassified by every model in an ensemble of models. We can denote the set of ViTs in the ensemble as $v \in V$ and the non-ViT models as $k \in K$. The adversary is assumed to have white-box capabilities (i.e., knowledge of the models and trained parameters of each model). The adversarial example is then computed over a fixed number of iterations as:

$$x_{adv}^{(i+1)} = x_{adv}^{(i)} + \epsilon_s * \text{sign}(G_{blend}(x_{adv}^{(i)})) \quad (12)$$

where $x_{adv}^{(1)} = x$ and ϵ_s is the step size for each iteration of the attack. The difference between a single model attack

like PGD and SAGA lies in the value of $G_{blend}(x_{adv}^{(i)})$:

$$G_{blend}(x_{adv}^{(i)}) = \sum_{k \in K} \alpha_k \frac{\partial L_k}{\partial x_{adv}^{(i)}} + \sum_{v \in V} \alpha_v \phi_v \odot \frac{\partial L_v}{\partial x_{adv}^{(i)}} \quad (13)$$

In Equation 13 the two summations represent the gradient contributions of the non-ViT and ViT sets K and V , respectively. For each ViT model v , $\frac{\partial L_v}{\partial x_{adv}^{(i)}}$ represents the partial derivative of the loss function with respect to the adversarial input $x_{adv}^{(i)}$. The term ϕ_v is the self-attention map [1] and α_v is the weighting factor associated with specific ViT model v . Likewise, for the first summation in In Equation 13 there is a partial derivative with respect to the loss function for the model and a weighting factor α_k for the given model k .

In practice using SAGA comes with significant drawbacks. Assume a model ensemble containing the set of

Algorithm 1 Auto Self-Attention Gradient Attack

- 1: **Input:** clean sample x , number of iterations N_{iter} , step size per iteration ϵ_{iter} , maximum perturbation ϵ_{max} , set of M models with corresponding loss functions L_1, \dots, L_M and coefficient learning rate r .
 - 2: **For** i in range 1 to N_{iter} do:
 - 3: *//Generate the adversarial example*
 - 4: $x_{adv}^{(i+1)} = x_{adv}^{(i)} + \epsilon_{step} \text{sign}(\sum_{m=1}^M \alpha_m^{(i)} \odot \frac{\partial L_m}{\partial x_{adv}^{(i)}} \odot \phi_m)$
 - 5: *//Apply projection operation*
 - 6: $x_{adv}^{i+1} = P(x_{adv}^{(i)}, x, \epsilon_{max})$
 - 7: **For** m in range 1 to M :
 - 8: *//Update the model coefficients*
 - 9: $\frac{\partial x_{adv}^{(i)}}{\partial \alpha_m^{(i)}} \approx u \epsilon_{step} \text{sech}^2(u \sum_{m=1}^M \frac{\partial L_m}{\partial x_{adv}^{(i)}}) \odot \frac{\partial L_m}{\partial x_{adv}^{(i)}}$
 - 10: $\frac{\partial F}{\partial \alpha_m^{(i)}} = \frac{\partial F}{\partial \alpha_{adv}^{(i)}} \odot \frac{\partial x_{adv}^{(i)}}{\partial \alpha_m^{(i)}}$
 - 11: $\alpha_m^{(i)} = \alpha_m^{(i)} - r \frac{\partial F}{\partial \alpha_m^{(i)}}$
 - 12: end for
 - 13: end for
 - 14: **Output:** x_{adv}
-

models $E = V \cup K$ and $|E| = M$. Every model m requires its own weighting factor such that $\overleftarrow{\alpha} = (\alpha_1, \dots, \alpha_m, \dots, \alpha_M)$. If these hyperparameters are not properly chosen, the attack performance of SAGA degrades significantly. This was first demonstrated in [30] when equal weighting was given to all models. We also demonstrate examples of this in our appendix. The second drawback of SAGA is that once $\overleftarrow{\alpha}$ is chosen for the attack, it is fixed for every sample and for every iteration of the attack. This makes choosing $\overleftarrow{\alpha}$ incredibly challenging as the hyperparameters values must either perform well for the majority of samples or have to be manually selected on a per sample basis.

5.2. Auto-SAGA

To remedy the shortcomings of SAGA, we propose Auto-SAGA, an enhanced version of SAGA that automatically derives the appropriate weighting factors $\overleftarrow{\alpha}$ in every iteration of the attack. The purpose of synthesizing this attack in our paper is two-fold: First we use Auto-SAGA to demonstrate that a white-box defense composed of a combination of SNNs, ViTs or CNNs is not robust. The second purpose of developing Auto-SAGA is to reduce the number of manually selected hyperparameters required by the original SAGA while increasing the success rate of the attack. The pseudo-code for Auto-SAGA is given in Algorithm 1. In principle Auto-SAGA works similarly to SAGA where in each iteration of the attack, the adversarial example is

| S-V-T5 | S-R-BP | C-V | V-L16 | C152x4-512 |
|--------|--------|--------|--------|------------|
| 57.53% | 60.82% | 71.59% | 82.94% | 85.31% |

Table 8. Clean Accuracy for ImageNet models

updated:

$$x_{adv}^{(i+1)} = x_{adv}^{(i)} + \epsilon_{step} \text{sign}(\sum_{m=1}^M \alpha_m^{(i)} \odot \frac{\partial L_m}{\partial x_{adv}^{(i)}} \odot \phi_m) \quad (14)$$

In Equation 14 the attention roll out ϕ_m is computed based on the model type:

$$\phi_m = \begin{cases} (\prod_{l=1}^{n_l} [\sum_{i=1}^{n_h} (0.5W_{l,i}^{(att)} + 0.5I)]) \odot x. & \text{If } m \in V, \\ J & \text{otherwise.} \end{cases} \quad (15)$$

where x is the input to the model, I is the identity matrix, $W_{l,i}^{(att)}$ is the attention weight matrix in each attention head, n_h is the number of attention heads per layer and n_l is the number of attention layers [1]. In the case when the model is not a Vision Transformer, the attention roll out is simply the ones matrix J . This distinction makes our attack suitable for attacking both ViT and non-ViT models.

After the adversarial example is computed, Auto-SAGA updates the weighting coefficients $\alpha_1, \dots, \alpha_m$ of each model to adjust the gradient computations for the next iteration:

$$\alpha_m^{(i)} = \alpha_m^{(i)} - r \frac{\partial F}{\partial \alpha_m^{(i)}} \quad (16)$$

where r is the learning rate for the coefficients and the effectiveness of the coefficients is measured and updated based on a modified version of the non-targeted loss function proposed in [5]:

$$F(x_{adv}^{(i)}) = \max(\max\{s(x_{adv}^{(i)})_j : j \neq t\} - s(x_{adv}^{(i)})_t, -\kappa) \quad (17)$$

where $s(\cdot)_j$ represents the j^{th} softmax output (probability) from the model, $s(\cdot)_t$ represents the softmax probability of the correct class label t and κ represents confidence with which the adversarial example should be misclassified (in our attacks we use $\kappa = 0$). Equation 16 can be computed by expanding $\frac{\partial F}{\partial \alpha_m^{(i)}} = \frac{\partial F}{\partial \alpha_{adv}^{(i)}} \odot \frac{\partial x_{adv}^{(i)}}{\partial \alpha_m^{(i)}}$ and approximating the derivative of $\text{sign}(x)$ in Equation 14 with $u \cdot \text{sech}^2(ux)$:

$$\frac{\partial x_{adv}^{(i)}}{\partial \alpha_m^{(i)}} \approx u \epsilon_{step} \text{sech}^2(u \sum_{m=1}^M \frac{\partial L_m}{\partial x_{adv}^{(i)}}) \odot \frac{\partial L_m}{\partial x_{adv}^{(i)}} \quad (18)$$

where u is a fitting factor for the derivative approximation.

5.3. Auto-SAGA Experimental Results

Experimental Setup: To evaluate the attack performance of Auto-SAGA, we conducted experiments on the

| Dataset | CIFAR-10 | | | | CIFAR-100 | | | | ImageNet | |
|-----------|----------|--------|---------|--------|-----------|--------|---------|--------|----------|--------|
| Model | S-R-BP | S-V-BP | S-V-T10 | S-V-T5 | S-R-BP | S-V-BP | S-V-T10 | S-V-T5 | S-R-BP | S-V-T5 |
| Timesteps | 4 | 20 | 10 | 5 | 5 | 30 | 10 | 5 | 4 | 5 |

Table 9. The timesteps used for each SNN model we used in the paper

| Model 1 | Model 2 | Max MIM | Max PGD | Basic SAGA | Auto SAGA |
|---------|---------|---------|---------|------------|--------------|
| C-V | S-R-BP | 18.5% | 16.1% | 26.6% | 90.4% |
| C-V | S-V-BP | 72.7% | 74.3% | 81.4% | 99.5% |
| C-V | S-V-T10 | 88.6% | 89.2% | 87.2% | 90.6% |
| C-V | S-R-T10 | 86.6% | 87.3% | 77.3% | 91.4% |
| S-R-BP | S-V-T10 | 15.3% | 13.4% | 18.4% | 61.6% |
| V-L16 | S-R-BP | 12.5% | 10.7% | 23.9% | 93.8% |
| V-L16 | S-V-BP | 10.7% | 7.1% | 52.4% | 73.2% |
| V-L16 | S-V-T10 | 9.5% | 4.8% | 28.4% | 92.7% |
| V-L16 | S-R-T10 | 16.0% | 7.7% | 36.6% | 99.0% |
| C-101x3 | S-R-BP | 17.3% | 14.3% | 58.7% | 80.5% |
| C-101x3 | S-V-BP | 15.3% | 8.9% | 31.6% | 83.8% |
| C-101x3 | S-V-T10 | 22.2% | 15.2% | 30.2% | 98.0% |
| C-101x3 | S-R-T10 | 25.4% | 16.8% | 62.3% | 98.8% |

Table 10. Attack Success Rate for CIFAR-10. Max MIM and PGD represent the max success rate using AEs generated by model 1 and model 2. Basic SAGA use coefficient [0.5, 0.5].

| Model 1 | Model 2 | Max MIM | Max PGD | Basic SAGA | Auto SAGA |
|---------|---------|---------|---------|------------|--------------|
| C-V | S-R-BP | 40.7% | 33.6% | 49.8% | 93.2% |
| C-V | S-V-BP | 59.4% | 51.3% | 67.2% | 94.7% |
| C-V | S-V-T10 | 73.1% | 68.6% | 78.6% | 84.0% |
| C-V | S-R-T10 | 69.6% | 46.6% | 84.4% | 91.8% |
| S-R-BP | S-V-T10 | 41.7% | 33.7% | 45.3% | 64.3% |
| V-L16 | S-R-BP | 28.3% | 23.5% | 74.5% | 78.9% |
| V-L16 | S-V-BP | 33.9% | 20.3% | 70.0% | 85.4% |
| V-L16 | S-V-T10 | 25.7% | 15.3% | 33.0% | 91.5% |
| V-L16 | S-R-T10 | 27.2% | 17.4% | 60.8% | 93.8% |
| C-101x3 | S-R-BP | 38.3% | 32.6% | 52.0% | 77.3% |
| C-101x3 | S-V-BP | 22.7% | 16.9% | 57.0% | 83.8% |
| C-101x3 | S-V-T10 | 24.6% | 20.3% | 44.5% | 84.5% |
| C-101x3 | S-R-T10 | 25.2% | 21.0% | 85.8% | 97.0% |

Table 11. Attack Success Rate for CIFAR-100. Max MIM and PGD represent the max success rate using AEs generated by model 1 and model 2. Basic SAGA use coefficient [0.5, 0.5].

CIFAR-10 and CIFAR-100 [21] datasets for the models introduced in Section 4. We test 13 different pairs of models that have low transferability. We further conduct experiments on 7 pairs of models for ImageNet [22]. For the ImageNet models we include the Vision Transformer (V-L16), Big Transfer CNN (C152x4-512) with corresponding input image size 512 and VGG-16 (C-V). We also use a BP trained SNN ResNet-18 (S-R-BP) [13] and a VGG-16 Transfer-based SNN (S-V-T5) [34] for attack capability exploration. The clean accuracies of the used models are listed in Table 5 for the CIFAR datasets and Table 8 for the ImageNet dataset. The detailed timesteps used for each SNN model are provided in Table 9. To attack each pair, we use 1000 correctly identified class-wise balanced samples from the validation set. For the attack, we use a maximum perturbation of $\epsilon = 0.031$ for CIFAR datasets and $\epsilon = 0.062$ for ImageNet with respect to the l_∞ norm. We compare Auto-

SAGA to the single MIM and single PGD attack with the highest attack success rate on each pair of models, we denote this type of attack as ‘‘Max MIM’’ and ‘‘Max PGD’’. We also compare Auto-SAGA to a balanced version of SAGA that uses model coefficients $\alpha_1 = \alpha_2 = 0.5$. All attacks use the arctan surrogate gradient estimation technique.

1. For single MIM and PGD attacks, we use $\epsilon_{step} = 0.01$, attack step = 40 to generate AEs from each model, and list the highest attack success rate on each pair of the models.
2. For basic SAGA, we set the attack as a balanced version of SAGA that uses coefficients $\alpha_1 = \alpha_2 = 0.5$ for two models to generate AEs and get the attack success rate among both models.
3. As for Auto-SAGA, we set learning rate $r = 10,000$ for the coefficients. We set attack step = 40 and $\epsilon_{step} = 0.005$ to generate AEs.

Lastly, it is important to note that we define the attack success rate as the percent of adversarial examples that are misclassified by *both* models in the pair of models.

Experimental Analysis: In Table 10 and Table 11 we attack 13 different pairs of models and report the resulting attack success rate. Overall, Auto-SAGA always gives the highest attack success rate among all tested attacks for each pair. For the pairings of models there are several novel findings. For pairs that contain a Vision Transformer and SNN, Auto-SAGA performs well even when all other attacks don’t. For example, for CIFAR-10 for ViT-L-16 (V-L16) and the SEW ResNet (S-R-BP) the best non-SAGA result only achieves an attack success rate of 12.5% but Auto-SAGA can achieve an attack success rate of 93.8%. For pairs that contain a CNN and corresponding Transfer SNN (which uses the CNN weights as a starting point), even MIM and PGD work well. For example, consider the pair: CNN VGG-16 (C-V) and the Transfer SNN VGG-16 (S-V-T10). For CIFAR-10 MIM gives an attack success rate of 88.6% and Auto-SAGA gives 90.6%. This shared vulnerability likely arises from the shared model weights. Lastly, the basic SAGA attack can learn gradient information from both models and in general it generates better adversarial examples better than MIM or PGD attacks. However, its performance is still much worse than Auto-SAGA. For example, Auto-SAGA has an average attack success rate improvement of 41.4% over standard SAGA for the CIFAR-10 pairs we tested.

| Model 1 | Model 2 | Max MIM | Max PGD | Basic SAGA | Auto SAGA |
|------------|---------|---------|---------|------------|----------------|
| C-V | S-R-BP | 83.60% | 70.80% | 95.30% | 99.70% |
| C-V | S-V-T5 | 87.70% | 79.20% | 98.60% | 100.00% |
| S-R-BP | S-V-T5 | 91.40% | 85.20% | 99.70% | 100.00% |
| V-L16 | S-R-BP | 66.10% | 41.80% | 73.70% | 97.30% |
| V-L16 | S-V-T5 | 65.30% | 42.10% | 78.40% | 98.80% |
| C152x4-512 | S-R-BP | 30.80% | 23.40% | 89.20% | 99.90% |
| C152x4-512 | S-V-T5 | 34.00% | 26.80% | 97.30% | 99.90% |

Table 12. Attack Success Rate for ImageNet. Max MIM and PGD represent the max success rate using AEs generated by model 1 and model 2. Basic SAGA use coefficient [0.5, 0.5].

In Table 12 we attack 7 different pairs of models and report the attack success rate for ImageNet task. Overall, our Auto-SAGA performance for ImageNet shows a similar trend to CIFAR, with higher attack success rates on most pairs due to the complexity of the ImageNet classification task (97.3% ~ 100%). One difference on ImageNet is that the attack shows great transferability between different kinds of SNNs. Even MIM and PGD attacks can achieve attack success rates of 91.40% and 85.20%, compared to 41.7% and 33.7% on CIFAR-100 task. This could result from similar timesteps (4 for REW ResNet and 5 for VGG) used for ImageNet SNN models, the complexity of the task, and the larger attack space due to larger image size.

6. Conclusion

Developments in BP SNNs and Transfer SNNs create new opportunities for energy efficient classifiers but also raise important security questions. In this paper, we investigated and analyzed three important aspects of SNN adversarial machine learning. First, we analyzed how the surrogate gradient estimator effects adversarial SNN attacks. We showed this choice plays a critical role in achieving a high attack success rate on both BP and Transfer SNNs.

Second, we used the best gradient estimator to create adversarial examples with different SNN models to measure their transferability with respect to state-of-the-art architectures like Visions Transformers and Big Transfer CNNs. We showed there exist multiple SNN/ViT and SNN/CNN pairings that do not share the same set of vulnerabilities to traditional adversarial machine learning attacks. Lastly, we proposed a new attack, Auto-SAGA which achieves a high attack success rate against both SNNs and non-SNN models (ViTs and CNNs) simultaneously. Our work advances the field of SNNs and adversarial machine learning by demonstrating the proper surrogate gradient attack techniques, showing where SNN adversarial transferability exists and by developing a novel attack that works across SNN and non-SNN models.

References

[1] Samira Abnar and Willem Zuidema. Quantifying attention flow in transformers. In *Proceedings of the 58th Annual*

Meeting of the Association for Computational Linguistics, pages 4190–4197, 2020.

[2] Anish Athalye, Nicholas Carlini, and David Wagner. Obfuscated gradients give a false sense of security: Circumventing defenses to adversarial examples. In *Proceedings of the 35th International Conference on Machine Learning*, pages 274–283, 2018.

[3] Guillaume Bellec, Darjan Salaj, Anand Subramoney, Robert Legenstein, and Wolfgang Maass. Long short-term memory and learning-to-learn in networks of spiking neurons. *Advances in neural information processing systems*, 31, 2018.

[4] Yoshua Bengio, Nicholas Léonard, and Aaron Courville. Estimating or propagating gradients through stochastic neurons for conditional computation. *arXiv preprint arXiv:1308.3432*, 2013.

[5] Nicholas Carlini and David Wagner. Towards evaluating the robustness of neural networks. In *2017 IEEE Symposium on Security and Privacy (SP)*, pages 39–57. Ieee, 2017.

[6] Mike Davies, Narayan Srinivasa, Tsung-Han Lin, Gautham China, Yongqiang Cao, Sri Harsha Choday, Georgios Dimou, Prasad Joshi, Nabil Imam, Shweta Jain, et al. Loihi: A neuromorphic manycore processor with on-chip learning. *Ieee Micro*, 38(1):82–99, 2018.

[7] Mike Davies, Andreas Wild, Garrick Orchard, Yulia Sandamirskaya, Gabriel A Fonseca Guerra, Prasad Joshi, Philipp Plank, and Sumedh R Risbud. Advancing neuromorphic computing with loihi: A survey of results and outlook. *Proceedings of the IEEE*, 109(5):911–934, 2021.

[8] Peter U Diehl, Daniel Neil, Jonathan Binas, Matthew Cook, Shih-Chii Liu, and Michael Pfeiffer. Fast-classifying, high-accuracy spiking deep networks through weight and threshold balancing. In *2015 International joint conference on neural networks (IJCNN)*, pages 1–8. IEEE, 2015.

[9] Yinpeng Dong, Fangzhou Liao, Tianyu Pang, Hang Su, Jun Zhu, Xiaolin Hu, and Jianguo Li. Boosting adversarial attacks with momentum. In *Proceedings of the IEEE conference on computer vision and pattern recognition (CVPR)*, pages 9185–9193, 2018.

[10] Alexey Dosovitskiy, Lucas Beyer, Alexander Kolesnikov, Dirk Weissenborn, Xiaohua Zhai, Thomas Unterthiner, Mostafa Dehghani, Matthias Minderer, Georg Heigold, Sylvain Gelly, et al. An image is worth 16x16 words: Transformers for image recognition at scale. In *International Conference on Learning Representations*, 2020.

[11] Rida El-Allami, Alberto Marchisio, Muhammad Shafique, and Ihsen Alouani. Securing deep spiking neural networks against adversarial attacks through inherent structural parameters. In *2021 Design, Automation & Test in Europe Conference & Exhibition (DATE)*, pages 774–779. IEEE, 2021.

[12] Haowen Fang, Zaidao Mei, Amar Shrestha, Ziyi Zhao, Yilan Li, and Qinru Qiu. Encoding, model, and architecture: Systematic optimization for spiking neural network in fpgas. In *2020 IEEE/ACM International Conference On Computer Aided Design (ICCAD)*, pages 1–9. IEEE, 2020.

[13] Haowen Fang, Amar Shrestha, Ziyi Zhao, and Qinru Qiu. Exploiting neuron and synapse filter dynamics in spatial temporal learning of deep spiking neural network. In *29th International Joint Conference on Artificial Intelligence, IJCAI*

- 2020, pages 2799–2806. International Joint Conferences on Artificial Intelligence, 2020.
- [14] Wei Fang, Zhaofei Yu, Yanqi Chen, Tiejun Huang, Timothée Masquelier, and Yonghong Tian. Deep residual learning in spiking neural networks. *Advances in Neural Information Processing Systems*, 34:21056–21069, 2021.
- [15] Wei Fang, Zhaofei Yu, Yanqi Chen, Timothée Masquelier, Tiejun Huang, and Yonghong Tian. Incorporating learnable membrane time constant to enhance learning of spiking neural networks. In *Proceedings of the IEEE/CVF International Conference on Computer Vision*, pages 2661–2671, 2021.
- [16] Ian Goodfellow, Jonathon Shlens, and Christian Szegedy. Explaining and harnessing adversarial examples. In *International Conference on Learning Representations*, 2015.
- [17] Ian J Goodfellow, Jonathon Shlens, and Christian Szegedy. Explaining and harnessing adversarial examples. *arXiv preprint arXiv:1412.6572*, 2014.
- [18] Kaiming He, Xiangyu Zhang, Shaoqing Ren, and Jian Sun. Deep residual learning for image recognition. In *Proceedings of the IEEE conference on computer vision and pattern recognition*, pages 770–778, 2016.
- [19] Mark Horowitz. 1.1 computing’s energy problem (and what we can do about it). In *2014 IEEE International Solid-State Circuits Conference Digest of Technical Papers (ISSCC)*, pages 10–14. IEEE, 2014.
- [20] Alexander Kolesnikov, Lucas Beyer, Xiaohua Zhai, Joan Puigcerver, Jessica Yung, Sylvain Gelly, and Neil Houlsby. Big transfer (bit): General visual representation learning. *Lecture Notes in Computer Science*, page 491–507, 2020.
- [21] Alex Krizhevsky, Geoffrey Hinton, et al. Learning multiple layers of features from tiny images. 2009.
- [22] Alex Krizhevsky, Ilya Sutskever, and Geoffrey E Hinton. Imagenet classification with deep convolutional neural networks. In *Advances in neural information processing systems*, pages 1097–1105, 2012.
- [23] Alexander Kugele, Thomas Pfeil, Michael Pfeiffer, and Elisabetta Chicca. Efficient processing of spatio-temporal data streams with spiking neural networks. *Frontiers in Neuroscience*, 14:439, 2020.
- [24] Souvik Kundu, Massoud Pedram, and Peter A Beerel. Hire-snn: Harnessing the inherent robustness of energy-efficient deep spiking neural networks by training with crafted input noise. In *Proceedings of the IEEE/CVF International Conference on Computer Vision*, pages 5209–5218, 2021.
- [25] Ling Liang, Xing Hu, Lei Deng, Yujie Wu, Guoqi Li, Yufei Ding, Peng Li, and Yuan Xie. Exploring adversarial attack in spiking neural networks with spike-compatible gradient. *IEEE transactions on neural networks and learning systems*, 2021.
- [26] Yanpei Liu, Xinyun Chen, Chang Liu, and Dawn Song. Delving into transferable adversarial examples and black-box attacks. *arXiv preprint arXiv:1611.02770*, 2016.
- [27] Sen Lu and Abhronil Sengupta. Exploring the connection between binary and spiking neural networks. *Frontiers in Neuroscience*, 14:535, 2020.
- [28] Aleksander Madry, Aleksandar Makelov, Ludwig Schmidt, Dimitris Tsipras, and Adrian Vladu. Towards deep learning models resistant to adversarial attacks. In *International Conference on Learning Representations*, 2018.
- [29] K Mahmood, D Gurevin, M van Dijk, and PH Nguyen. Beware the black-box: On the robustness of recent defenses to adversarial examples. *Entropy*, 23:1359, 2021.
- [30] Kaleel Mahmood, Rigel Mahmood, and Marten Van Dijk. On the robustness of vision transformers to adversarial examples. In *Proceedings of the IEEE/CVF International Conference on Computer Vision*, pages 7838–7847, 2021.
- [31] Kaleel Mahmood, Phuong Ha Nguyen, Lam M. Nguyen, Thanh Nguyen, and Marten Van Dijk. Besting the black-box: Barrier zones for adversarial example defense. *IEEE Access*, 10:1451–1474, 2022.
- [32] Emre O Neftci, Hesham Mostafa, and Friedemann Zenke. Surrogate gradient learning in spiking neural networks: Bringing the power of gradient-based optimization to spiking neural networks. *IEEE Signal Processing Magazine*, 36(6):51–63, 2019.
- [33] Nicolas Papernot, Patrick McDaniel, and Ian Goodfellow. Transferability in machine learning: from phenomena to black-box attacks using adversarial samples. *arXiv preprint arXiv:1605.07277*, 2016.
- [34] Nitin Rathi and Kaushik Roy. Diet-snn: A low-latency spiking neural network with direct input encoding and leakage and threshold optimization. *IEEE Transactions on Neural Networks and Learning Systems*, 2021.
- [35] Nitin Rathi, Gopalakrishnan Srinivasan, Priyadarshini Panda, and Kaushik Roy. Enabling deep spiking neural networks with hybrid conversion and spike timing dependent backpropagation. In *International Conference on Learning Representations*, 2020.
- [36] Bodo Rueckauer, Connor Bybee, Ralf Goetsche, Yashwardhan Singh, Joyesh Mishra, and Andreas Wild. Nxtf: An api and compiler for deep spiking neural networks on intel loihi. *ACM Journal on Emerging Technologies in Computing Systems (JETC)*, 18(3):1–22, 2022.
- [37] Saima Sharmin, Priyadarshini Panda, Syed Shakib Sarwar, Chankyu Lee, Wachirawit Ponghiran, and Kaushik Roy. A comprehensive analysis on adversarial robustness of spiking neural networks. In *2019 International Joint Conference on Neural Networks (IJCNN)*, pages 1–8. IEEE, 2019.
- [38] Saima Sharmin, Nitin Rathi, Priyadarshini Panda, and Kaushik Roy. Inherent adversarial robustness of deep spiking neural networks: Effects of discrete input encoding and non-linear activations. In *European Conference on Computer Vision*, pages 399–414. Springer, 2020.
- [39] Amar Shrestha, Haowen Fang, Zaidao Mei, Daniel Patrick Rider, Qing Wu, and Qinru Qiu. A survey on neuromorphic computing: Models and hardware. *IEEE Circuits and Systems Magazine*, 22(2):6–35, 2022.
- [40] Sumit B Shrestha and Garrick Orchard. Slayer: Spike layer error reassignment in time. *Advances in neural information processing systems*, 31, 2018.
- [41] Karen Simonyan and Andrew Zisserman. Very deep convolutional networks for large-scale image recognition. *arXiv preprint arXiv:1409.1556*, 2014.
- [42] Christian Szegedy, Wojciech Zaremba, Ilya Sutskever, Joan Bruna, Dumitru Erhan, Ian Goodfellow, and Rob Fergus.

- Intriguing properties of neural networks. *arXiv preprint arXiv:1312.6199*, 2013.
- [43] Guangzhi Tang, Neelesh Kumar, and Konstantinos P Michmizos. Reinforcement co-learning of deep and spiking neural networks for energy-efficient mapless navigation with neuro-morphic hardware. In *2020 IEEE/RSJ International Conference on Intelligent Robots and Systems (IROS)*, pages 6090–6097. IEEE, 2020.
 - [44] Amirhossein Tavanaei, Masoud Ghodrati, Saeed Reza Kheradpisheh, Timothée Masquelier, and Anthony Maida. Deep learning in spiking neural networks. *Neural networks*, 111:47–63, 2019.
 - [45] Florian Tramer, Nicholas Carlini, Wieland Brendel, and Aleksander Madry. On adaptive attacks to adversarial example defenses. *Advances in Neural Information Processing Systems*, 33:1633–1645, 2020.
 - [46] Yujie Wu, Lei Deng, Guoqi Li, Jun Zhu, and Luping Shi. Spatio-temporal backpropagation for training high-performance spiking neural networks. *Frontiers in neuroscience*, 12:331, 2018.
 - [47] Yujie Wu, Lei Deng, Guoqi Li, Jun Zhu, Yuan Xie, and Luping Shi. Direct training for spiking neural networks: Faster, larger, better. In *Proceedings of the AAAI Conference on Artificial Intelligence*, volume 33, pages 1311–1318, 2019.
 - [48] Friedemann Zenke and Surya Ganguli. Superspike: Supervised learning in multilayer spiking neural networks. *Neural computation*, 30(6):1514–1541, 2018.
 - [49] Friedemann Zenke and Tim P Vogels. The remarkable robustness of surrogate gradient learning for instilling complex function in spiking neural networks. *Neural computation*, 33(4):899–925, 2021.
 - [50] Jingfeng Zhang, Xilie Xu, Bo Han, Gang Niu, Lizhen Cui, Masashi Sugiyama, and Mohan Kankanhalli. Attacks which do not kill training make adversarial learning stronger. In *International conference on machine learning*, pages 11278–11287. PMLR, 2020.
 - [51] Wenrui Zhang and Peng Li. Temporal spike sequence learning via backpropagation for deep spiking neural networks. *Advances in Neural Information Processing Systems*, 33:12022–12033, 2020.
 - [52] Hanle Zheng, Yujie Wu, Lei Deng, Yifan Hu, and Guoqi Li. Going deeper with directly-trained larger spiking neural networks. In *Proceedings of the AAAI Conference on Artificial Intelligence*, volume 35, pages 11062–11070, 2021.

A. SNN Energy Efficiency

| Architecture | Dataset | Normalized ANN #OP | Normalized SNN #OP | ANN/SNN Energy |
|-------------------------|-----------|--------------------|--------------------|----------------|
| SEW-ResNet | CIFAR 10 | 1 | 0.4052 | 12.61 |
| SEW-ResNet | CIFAR 100 | 1 | 0.5788 | 8.83 |
| SEW-ResNet | ImageNet | 1 | 0.5396 | 9.47 |
| Vanilla Spiking ResNet | ImageNet | 1 | 0.6776 | 7.54 |
| Transfer Spiking VGG 16 | ImageNet | 1 | 2.868 | 1.78 |

Table 13. ANN and SNN energy consumption.

Benefiting from the binary spikes, the expensive multiplication in DNNs can be greatly eliminated in SNNs. We followed the methodology in [34] and energy model in [19, 34] to theoretically analyze the energy efficiency of SNNs used in this work. For each 32-bit Multiply-Accumulate Operation (MAC) in ANN, energy cost is $4.6pJ$ [19]. One MAC of ANN is equivalent to multiple Addition-Accumulation Operations (AAC) of SNN in a time window T , number of AAC is calculated as $\#OP_{SNN} = SpikeRate \times T$. Each AAC takes $0.9pJ$ energy. Theoretical comparison is shown in Table 13. ANNs consume 1.78-12.61 times more energy than SNNs. Note that the actual energy efficiency is technology and implementation dependent, and this theoretical calculation is pessimistic: other factors such as data movement, architectural design, etc., which also contribute to neuromorphic chips energy efficiency, are not taken into account. As mentioned in Section 1, various works have reported $10 \times -276 \times$ energy efficiency over CPU/GPU with dedicated off-the-shelf neuromorphic chips.

B. White-Box Attacks Appendix

B.1. Fast Gradient Sign Method

The Fast Gradient Sign Method (FGSM) [16] is a white box attack that generates adversarial examples by adding noise to the clean image in the direction of the gradients of the loss function:

$$x_{adv} = x + \epsilon \cdot \text{sign}(\Delta_x L(x, y; \theta)) \quad (19)$$

where ϵ is the attack step size parameter and L is the loss function of the targeted model. The attack performs only a single step of perturbation, and applies noise in the direction of the sign of the gradient of the model’s loss function.

B.2. Projected Gradient Descent

The Projected Gradient Descent attack (PGD) [28] is a modified version of the FGSM attack that implements multiple attack steps. The attack attempts to find the minimum

perturbation, bounded by ϵ , which maximizes the model’s loss for a particular input, x . The attack begins by generating a random perturbation on a ball centered at x and with radius ϵ . Adding this noise to x gives the initial adversarial input, x_0 . From here the attack begins an iterative process that runs for k steps. During the i^{th} attack step the perturbed image, x_i , is updated as follows:

$$x_i = P(x_{i-1} + \alpha \cdot \text{sign}(\Delta_x L(x_{i-1}, y; \theta))) \quad (20)$$

where P is a function that projects the adversarial input back onto the ϵ -ball in the case where it steps outside the bounds of the ball and α is the attack step size. The bounds of the ball are defined by the l_p norm.

B.3. Momentum Iterative Method

The Momentum Iterative Method (MIM) [9] applies momentum techniques seen in machine learning training to the domain of adversarial machine learning. Similar to those learning methods, the MIM attack’s momentum allows it to overcome local minima and maxima. The attack’s main formulation is similar to the formulation seen in the PGD attack. Each attack iteration is calculated as follows:

$$x_i = \text{clip}_{x, \epsilon} (x_{i-1} + \frac{\epsilon}{t} \cdot \text{sign}(g_i)) \quad (21)$$

where x_i represents the adversarial input at iteration i , ϵ is the total attack magnitude, and t is the total number of attack iterations. g_i represents the accumulated gradient at step i and is calculated as follows:

$$g_i = \mu \cdot g_{i-1} + \frac{\Delta_x L(x_{i-1}, y; \theta)}{\|\Delta_x L(x_{i-1}, y; \theta)\|_1} \quad (22)$$

where μ represents a momentum decay factor. Due to its similarity of formulation, the MIM attack degenerates to an iterative form of FGSM as μ approaches 0.

C. SNN Transferability Study Appendix

| FGSM | | | | | | | | | | | | |
|---------|--------|--------|--------|---------|--------|---------|---------|-------|-------|-------|-------|-------|
| | S-R-BP | S-V-BP | S-V-T5 | S-V-T10 | S-R-T5 | S-R-T10 | C-101x3 | C-V | C-R | V-B32 | V-B16 | V-L16 |
| S-R-BP | 48.1% | 17.1% | 14.6% | 14.7% | 18.2% | 15.9% | 3.4% | 11.8% | 15.5% | 5.2% | 4.9% | 2.9% |
| S-V-BP | 14.2% | 48.2% | 33.3% | 35.0% | 39.5% | 37.7% | 7.6% | 32.2% | 39.6% | 7.6% | 6.4% | 4.4% |
| S-V-T5 | 17.6% | 36.8% | 50.8% | 63.2% | 47.4% | 48.2% | 11.5% | 63.1% | 47.8% | 9.5% | 11.2% | 6.5% |
| S-V-T10 | 16.3% | 38.6% | 67.4% | 49.2% | 45.5% | 47.1% | 10.3% | 62.9% | 50.3% | 8.7% | 11.4% | 7.4% |
| S-R-T5 | 10.3% | 30.9% | 32.2% | 33.6% | 48.2% | 62.8% | 8.9% | 31.7% | 57.3% | 6.3% | 6.8% | 4.9% |
| S-R-T10 | 11.9% | 32.4% | 40.1% | 43.1% | 68.6% | 56.7% | 13.0% | 41.3% | 67.9% | 8.8% | 9.3% | 6.9% |
| C-101x3 | 8.4% | 4.8% | 3.7% | 2.7% | 7.0% | 3.6% | 13.6% | 1.6% | 2.2% | 3.4% | 6.2% | 4.6% |
| C-V | 18.2% | 45.2% | 66.8% | 70.3% | 54.7% | 55.9% | 16.1% | 55.6% | 54.9% | 13.2% | 14.5% | 10.8% |
| C-R | 15.5% | 50.8% | 58.1% | 60.1% | 80.8% | 82.7% | 17.6% | 61.0% | 70.9% | 14.6% | 16.0% | 11.8% |
| V-B32 | 8.7% | 9.6% | 9.8% | 9.1% | 14.9% | 12.6% | 27.4% | 8.3% | 12.4% | 57.4% | 44.0% | 35.2% |
| V-B16 | 6.1% | 8.9% | 7.2% | 5.9% | 10.5% | 6.9% | 23.7% | 4.9% | 7.1% | 31.1% | 59.7% | 41.0% |
| V-L16 | 7.6% | 6.9% | 7.7% | 5.7% | 8.8% | 8.6% | 20.7% | 6.2% | 7.4% | 23.8% | 37.7% | 38.5% |

| PGD | | | | | | | | | | | | |
|---------|--------|--------|--------|---------|--------|---------|---------|-------|-------|-------|-------|-------|
| | S-R-BP | S-V-BP | S-V-T5 | S-V-T10 | S-R-T5 | S-R-T10 | C-101x3 | C-V | C-R | V-B32 | V-B16 | V-L16 |
| S-R-BP | 63.3% | 21.2% | 18.4% | 17.9% | 22.2% | 17.9% | 4.4% | 14.1% | 18.6% | 5.8% | 5.2% | 4.2% |
| S-V-BP | 11.2% | 68.6% | 41.3% | 41.6% | 53.1% | 54.1% | 7.8% | 39.1% | 52.7% | 5.5% | 4.8% | 3.0% |
| S-V-T5 | 14.4% | 52.3% | 76.8% | 100.0% | 76.3% | 74.9% | 10.9% | 95.1% | 74.9% | 6.1% | 7.1% | 4.6% |
| S-V-T10 | 12.9% | 50.4% | 99.8% | 72.4% | 69.1% | 73.3% | 9.2% | 95.5% | 71.7% | 5.3% | 8.5% | 5.2% |
| S-R-T5 | 8.9% | 28.6% | 35.9% | 37.6% | 61.9% | 95.3% | 8.3% | 35.8% | 83.5% | 3.1% | 4.2% | 2.1% |
| S-R-T10 | 10.2% | 34.9% | 44.7% | 47.5% | 97.7% | 75.0% | 11.3% | 48.3% | 93.2% | 5.8% | 4.9% | 3.2% |
| C-101x3 | 16.2% | 70.8% | 92.7% | 93.7% | 84.5% | 86.4% | 26.9% | 89.3% | 85.7% | 18.7% | 21.7% | 14.6% |
| C-V | 13.4% | 65.5% | 77.6% | 77.1% | 98.1% | 97.7% | 30.6% | 78.0% | 92.9% | 18.7% | 20.7% | 13.4% |
| C-R | 6.4% | 3.5% | 3.3% | 2.4% | 6.4% | 3.8% | 100.0% | 1.0% | 2.1% | 2.1% | 2.8% | 0.7% |
| V-B32 | 6.1% | 6.5% | 6.0% | 5.1% | 11.9% | 6.6% | 30.5% | 4.5% | 5.3% | 97.1% | 60.7% | 35.5% |
| V-B16 | 5.9% | 5.6% | 4.6% | 3.6% | 7.3% | 3.6% | 17.4% | 1.5% | 2.7% | 13.7% | 99.6% | 56.4% |
| V-L16 | 6.9% | 5.6% | 5.2% | 3.6% | 7.0% | 5.8% | 21.5% | 2.4% | 2.9% | 18.2% | 77.8% | 92.8% |

| MIM | | | | | | | | | | | | |
|---------|--------|--------|--------|---------|--------|---------|---------|-------|-------|-------|-------|-------|
| | S-R-BP | S-V-BP | S-V-T5 | S-V-T10 | S-R-T5 | S-R-T10 | C-101x3 | C-V | C-R | V-B32 | V-B16 | V-L16 |
| S-R-BP | 69.2% | 23.7% | 19.5% | 19.9% | 26.1% | 22.4% | 5.3% | 18.0% | 21.6% | 7.5% | 6.1% | 4.4% |
| S-V-BP | 13.7% | 80.2% | 55.9% | 55.4% | 65.1% | 67.3% | 11.6% | 54.2% | 64.4% | 10.3% | 9.3% | 5.0% |
| S-V-T5 | 18.5% | 64.9% | 88.3% | 99.4% | 85.1% | 85.0% | 16.6% | 97.7% | 86.0% | 10.5% | 12.6% | 9.0% |
| S-V-T10 | 15.8% | 61.3% | 99.4% | 83.2% | 77.4% | 83.2% | 13.8% | 98.1% | 79.9% | 9.6% | 11.7% | 8.3% |
| S-R-T5 | 11.5% | 46.1% | 56.7% | 58.0% | 78.7% | 96.7% | 16.6% | 55.3% | 91.9% | 10.3% | 12.6% | 7.9% |
| S-R-T10 | 12.4% | 51.7% | 60.5% | 64.5% | 97.4% | 83.9% | 20.2% | 63.5% | 94.1% | 11.7% | 11.2% | 8.1% |
| C-101x3 | 18.1% | 71.3% | 90.1% | 91.4% | 82.7% | 85.4% | 25.7% | 87.8% | 84.5% | 20.9% | 22.8% | 16.2% |
| C-V | 16.4% | 70.2% | 82.3% | 80.3% | 96.7% | 96.5% | 31.6% | 81.0% | 92.3% | 23.0% | 27.2% | 17.5% |
| C-R | 6.2% | 4.7% | 4.4% | 3.6% | 8.8% | 6.0% | 100.0% | 2.5% | 3.8% | 8.5% | 21.5% | 11.5% |
| V-B32 | 8.8% | 10.9% | 10.8% | 11.2% | 15.9% | 12.7% | 58.7% | 9.2% | 13.5% | 95.2% | 85.3% | 72.7% |
| V-B16 | 6.7% | 6.5% | 7.5% | 6.0% | 10.6% | 7.2% | 41.4% | 4.9% | 6.9% | 56.7% | 98.2% | 87.5% |
| V-L16 | 6.7% | 8.2% | 7.6% | 6.7% | 11.2% | 9.2% | 45.4% | 6.5% | 8.4% | 54.4% | 77.7% | 85.7% |

Table 14. Full transferability results for CIFAR-10. The first column in each table represents the model used to generate the adversarial examples, C_i . The top row in each table represents the model used to evaluate the adversarial examples, C_j . Each entry represents $T_{i,j}$ (the transferability) computed using Equation 11 with C_i , C_j and either FGSM, PGD or MIM. For each attack the maximum perturbation bounds is $\epsilon = 0.031$. Based on these results we take the maximum transferability across all attacks and report the result in Table 6. We also visually show the maximum transferability $t_{i,j}$ in Figure 3.

| FGSM | | | | | | | | | | | |
|---------|--------|--------|--------|---------|--------|-------|-------|-------|-------|-------|---------|
| | S-R-BP | S-V-BP | S-V-T5 | S-V-T10 | S-R-T8 | V-B32 | V-B16 | V-L16 | C-V | C-R | C-101x3 |
| S-R-BP | 77.4% | 41.6% | 31.8% | 27.8% | 29.6% | 19.6% | 20.6% | 15.0% | 28.2% | 22.0% | 21.0% |
| S-V-BP | 40.4% | 50.0% | 35.8% | 40.0% | 39.4% | 11.0% | 12.4% | 9.8% | 35.2% | 31.8% | 14.4% |
| S-V-T5 | 35.8% | 50.2% | 60.4% | 83.6% | 57.2% | 18.6% | 19.2% | 10.4% | 76.6% | 52.6% | 16.8% |
| S-V-T10 | 37.4% | 56.2% | 82.0% | 57.2% | 48.0% | 15.6% | 13.6% | 12.0% | 75.8% | 44.2% | 16.6% |
| S-R-T8 | 30.6% | 44.8% | 47.0% | 44.6% | 70.8% | 11.4% | 13.0% | 7.4% | 40.0% | 64.0% | 12.0% |
| V-B32 | 35.8% | 20.4% | 17.0% | 11.2% | 19.2% | 77.4% | 61.4% | 54.4% | 12.2% | 12.0% | 42.6% |
| V-B16 | 25.2% | 17.2% | 10.2% | 8.8% | 17.2% | 49.8% | 77.4% | 60.8% | 8.4% | 5.4% | 43.0% |
| V-L16 | 28.8% | 20.4% | 12.0% | 10.6% | 17.6% | 42.6% | 55.4% | 60.4% | 9.0% | 7.8% | 41.4% |
| C-V | 41.6% | 56.8% | 79.4% | 80.2% | 57.8% | 26.6% | 22.6% | 16.6% | 61.2% | 53.6% | 21.0% |
| C-R | 39.0% | 53.6% | 58.2% | 56.8% | 76.8% | 21.2% | 16.8% | 14.2% | 56.6% | 88.8% | 18.0% |
| C-101x3 | 15.0% | 11.8% | 6.6% | 5.6% | 14.6% | 11.4% | 17.4% | 14.8% | 2.8% | 3.4% | 34.0% |

| PGD | | | | | | | | | | | |
|---------|--------|--------|--------|---------|--------|-------|-------|-------|-------|-------|---------|
| | S-R-BP | S-V-BP | S-V-T5 | S-V-T10 | S-R-T8 | V-B32 | V-B16 | V-L16 | C-V | C-R | C-101x3 |
| S-R-BP | 93.6% | 40.6% | 26.6% | 26.4% | 29.2% | 22.6% | 21.8% | 17.0% | 24.6% | 22.8% | 24.0% |
| S-V-BP | 35.2% | 55.8% | 32.8% | 34.0% | 32.0% | 8.4% | 10.4% | 7.0% | 35.4% | 30.8% | 11.4% |
| S-V-T5 | 27.2% | 47.2% | 65.2% | 97.2% | 59.6% | 10.8% | 13.2% | 9.0% | 92.8% | 55.4% | 15.8% |
| S-V-T10 | 28.4% | 53.0% | 96.8% | 64.0% | 54.0% | 10.2% | 10.2% | 8.4% | 93.0% | 51.6% | 14.4% |
| S-R-T8 | 28.6% | 58.8% | 72.2% | 71.0% | 99.0% | 14.6% | 15.4% | 9.6% | 68.2% | 94.4% | 15.2% |
| V-B32 | 13.8% | 14.0% | 9.2% | 7.4% | 15.8% | 97.4% | 74.2% | 57.6% | 6.2% | 6.6% | 35.8% |
| V-B16 | 9.4% | 12.4% | 7.8% | 6.4% | 14.4% | 31.6% | 99.8% | 78.6% | 3.2% | 2.6% | 22.8% |
| V-L16 | 7.4% | 16.6% | 8.8% | 6.6% | 15.2% | 36.2% | 86.0% | 95.6% | 3.4% | 2.4% | 33.0% |
| C-V | 42.6% | 64.0% | 90.4% | 91.8% | 66.4% | 26.6% | 23.0% | 16.0% | 77.4% | 66.2% | 25.8% |
| C-R | 37.6% | 56.8% | 61.8% | 64.6% | 92.8% | 17.0% | 16.0% | 11.6% | 69.2% | 98.6% | 18.0% |
| C-101x3 | 9.0% | 13.4% | 6.8% | 6.4% | 17.0% | 3.8% | 11.0% | 7.4% | 2.4% | 1.8% | 98.2% |

| MIM | | | | | | | | | | | |
|---------|--------|--------|--------|---------|--------|-------|-------|-------|-------|-------|---------|
| | S-R-BP | S-V-BP | S-V-T5 | S-V-T10 | S-R-T8 | V-B32 | V-B16 | V-L16 | C-V | C-R | C-101x3 |
| S-R-BP | 94.4% | 52.8% | 34.2% | 32.4% | 33.8% | 30.8% | 28.8% | 22.8% | 31.8% | 28.6% | 29.6% |
| S-V-BP | 48.8% | 66.6% | 47.2% | 49.0% | 51.0% | 18.2% | 21.2% | 14.4% | 48.8% | 42.2% | 18.4% |
| S-V-T5 | 37.8% | 60.0% | 76.4% | 97.4% | 69.4% | 18.8% | 19.8% | 13.0% | 93.0% | 64.4% | 20.8% |
| S-V-T10 | 36.0% | 60.0% | 95.4% | 72.0% | 60.6% | 15.6% | 14.8% | 13.2% | 92.4% | 57.0% | 19.8% |
| S-R-T8 | 41.8% | 65.4% | 76.4% | 76.4% | 98.8% | 18.6% | 22.8% | 13.4% | 73.6% | 95.4% | 18.6% |
| V-B32 | 28.2% | 21.4% | 15.4% | 14.0% | 19.4% | 96.6% | 89.2% | 81.2% | 12.8% | 10.8% | 58.8% |
| V-B16 | 17.6% | 18.6% | 11.0% | 8.2% | 16.6% | 73.2% | 99.2% | 94.4% | 5.8% | 6.0% | 48.6% |
| V-L16 | 20.4% | 17.8% | 11.6% | 8.0% | 16.4% | 66.2% | 86.0% | 93.0% | 6.0% | 6.4% | 53.2% |
| C-V | 44.6% | 66.8% | 90.2% | 91.6% | 69.4% | 30.0% | 24.8% | 19.0% | 78.0% | 69.0% | 26.8% |
| C-R | 41.6% | 59.2% | 65.6% | 67.6% | 92.8% | 23.4% | 19.8% | 16.2% | 71.0% | 97.6% | 19.0% |
| C-101x3 | 14.2% | 16.0% | 7.8% | 8.4% | 16.8% | 21.0% | 37.4% | 28.2% | 4.6% | 3.6% | 98.6% |

Table 15. Full transferability results for CIFAR-100. The first column in each table represents the model used to generate the adversarial examples, C_i . The top row in each table represents the model used to evaluate the adversarial examples, C_j . Each entry represents $T_{i,j}$ (the transferability) computed using Equation 11 with C_i , C_j and either FGSM, PGD or MIM. For each attack the maximum perturbation bounds is $\epsilon = 0.031$. Based on these results we take the maximum transferability across all attacks and report the result in Table 7. We also visually show the maximum transferability $t_{i,j}$ in Figure 4.